Delft University of Technology

CFD 3: LES Assignment 2

Delft University of Technology, Delft, South Holland, 2628 CD

Changkyu Park 4646061

Submission Date: April 7, 2021
Course: AE4139

Contents

1. Derivation of viscosity with respect to Reynolds number

Using a balance of forces F acting on the surface of the volume, viscosity ν can be expressed in terms of Re_τ. Since the blue volume as a whole does not have a net acceleration and thus for a net force, we have

$$\sum F = 0.$$

Since the 2-dimensional "volume" has 4 sides, we can rewrite the above equation as

$$F_{\text{left}} + F_{\text{right}} + F_{\text{top}} + F_{\text{bottom}} = 0.$$

With pressure forces p acting on the left and the right sides while viscous forces act on the top and the bottom sides, the above equation is then expanded to

$$\begin{aligned} p_{x=0} \cdot 2h + (-p_{x=L} \cdot 2h) + (-\tau_{\text{wall}} \cdot L) + (-\tau_{\text{wall}} \cdot L) &= 0 \\ 2h\left(p_{x=0} - p_{x=L}\right) - 2\tau_{\text{wall}} \cdot L &= 0. \end{aligned}$$

Using Stokes' theorem, the equation can be rewritten as

$$\begin{aligned} 2h \int_0^L \frac{dp}{dx}\, dx - 2\tau_{\text{wall}} \cdot L &= 0 \\ h \int_0^L \frac{dp}{dx}\, dx - \tau_{\text{wall}} \cdot L &= 0. \end{aligned}$$

Since the mean pressure gradient is given as $d\langle p \rangle / dx = 1$ and it can be used to describe dp/dx in the domain $x \in [0, L]$, the above equation is again rewritten as

$$\begin{aligned} h \int_0^L 1 dx - \tau_{\text{wall}} \cdot L &= 0 \\ hL - \tau_{\text{wall}} \cdot L &= 0 \\ \tau_{\text{wall}} &= h \\ &= 1 \end{aligned}$$

since $h = 1$. With $\tau_{\text{wall}} = 1$ and $\rho = 1$, for u_τ we have

$$\begin{aligned} u_\tau &= \sqrt{\frac{\tau_{\text{wall}}}{\rho}} \\ &= 1. \end{aligned} \tag{1.1}$$

Moreover, Re_τ is defined as

$$\begin{aligned} Re_\tau &= \frac{u_\tau h}{\nu} \\ &= \frac{u_\tau}{\nu} \end{aligned} \tag{1.2}$$

where

$$\begin{aligned} \nu &= \delta_\nu u_\tau \\ &= \delta_\nu. \end{aligned} \tag{1.3}$$

Substituting (1.1) into (1.2), we ultimately get

$$\begin{aligned} Re_\tau &= \frac{1}{\nu} \\ \boxed{\nu = \frac{1}{Re_\tau}}. \end{aligned} \tag{1.4}$$

2. Comparison between 32^3 mesh simulations

For the 32^3 mesh, simulations of 5 different cases were conducted and they are:

Case 1 : Constant-coefficient Smagorinsky, with $C_s = 0.065$ (low Re channel flow) and central flux evaluation
Case 2 : Constant-coefficient Smagorinsky, with $C_s = 0.17$ (isotropic flow) and central flux evaluation
Case 3 : Constant-coefficient Smagorinsky, with $C_s = 0.065$, central flux evaluation and Van Driest Damping
Case 4 : Constant-coefficient Smagorinsky, with $C_s = 0.065$ and upwind flux evaluation
Case 5 : Volume-averaged dynamic Smagorinsky with central flux evaluation

The plotted results of the simulations are shown in Figure 1 together with DNS results.

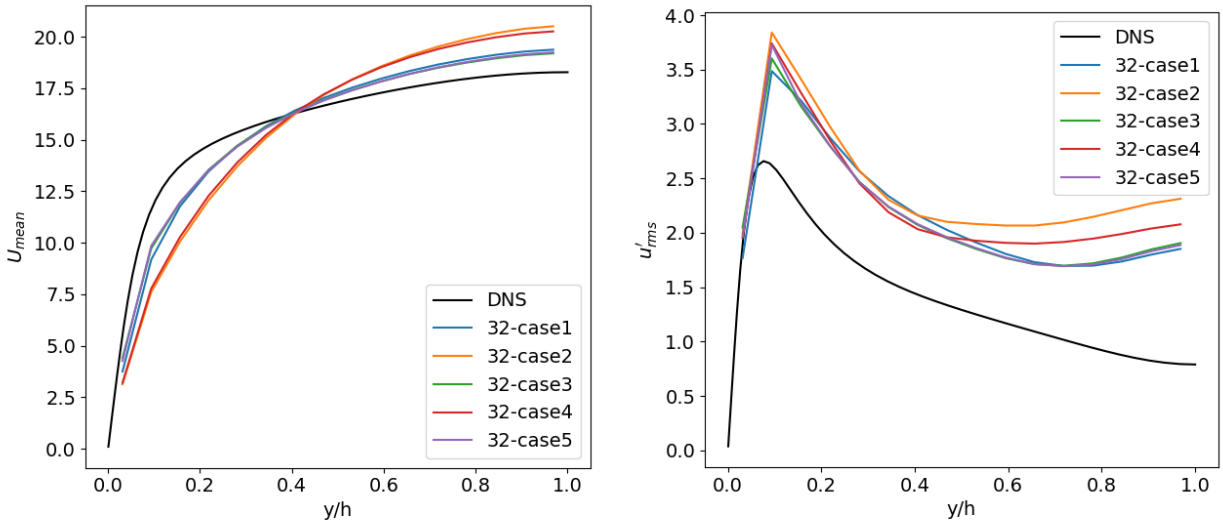

(a) $U_{\mathbf{mean}}$

(b) $u'_{\mathbf{rms}}$

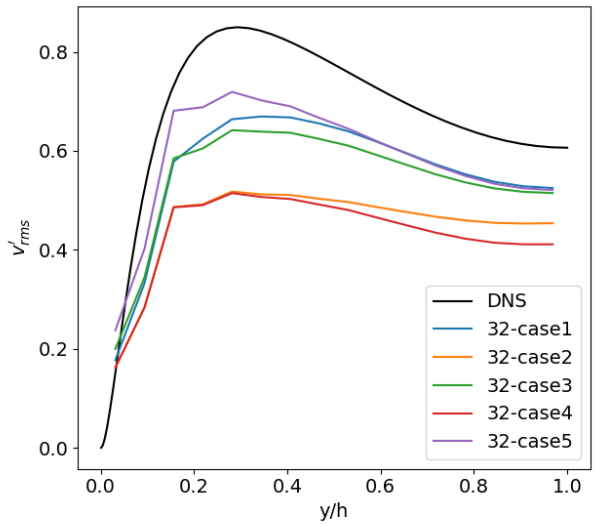

(c) $v'_{\mathbf{rms}}$

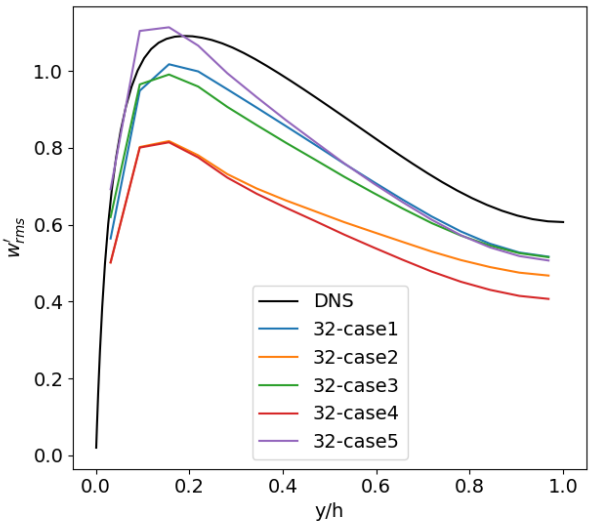

(d) $w'_{\mathbf{rms}}$

Fig. 1 Comparison of the 5 cases of 32^3 against DNS data for mean velocity and root-mean-square (rms) fluctuations

Starting with the observations from mean velocity featured in Figure 1a, it can be seen that cases 1,3 and 5 have highly identical results (green is almost completely overshadowed by purple) while cases 2 and 4 themselves also have very similar results that were relatively less accurate. These additional inaccuracies from case 2 and 4 are due to their simulation characteristics. Firstly for case 2, it uses Smagorinsky coefficient of $C_s = 0.17$ that corresponds to an isotropic flow to simulate a low Re channel flow which introduces more error than using $C_s = 0.065$ that fits this specific low Re channel flow that is the subject of this assignment. Secondly, for case 4, it uses an upwind flux evaluation that is of first-order thus is an order of accuracy lower than the other cases that utilise the second-order accurate central flux evaluation. Furthermore, it can also be realised that usages of Van driest damping and volume-averaged dynamic Smagorinsky have minimal effects on the accuracy for U_{mean}.

As for the plots of rms fluctuations in the flow direction presented in Figure 1b, it is observed that all 5 cases have similar results until $y/h = 0.4$ approximately. From this point, cases 1, 3 and 5 again features similar results while cases 2 and 4 deviate away from them with each having a slightly different magnitude of deviation. It can thus be inferred again that usages of Van driest damping and volume-averaged dynamic Smagorinsky have minimal effects on the accuracy for u'_{rms}. On the other hand, the usage of Smagorinsky coefficient of $C_s = 0.17$ has a greater adverse effect on the accuracy for u'_{rms} compared to the usage of the upwind scheme.

Behaviour of the results for the 5 cases are similar in both plots of rms fluctuations in v and w shown in Figure 1c and Figure 1d respectively. In these plots, the curves of case 5 seem to have deviated away from the curves of case 1 and 3, by approaching the DNS solution (black) more closely. This shows that the implementation of volume-averaged dynamic Smagorinsky model improves the results for rms fluctuations that are not in the flow direction, especially closer to the wall at low y/h.

Furthermore, cases 1 and 3 also show a slight difference in these plots with case 1 (blue) being more accurate in general. However, with closer inspection, it can be seen that case 3 (green) has a slightly better accuracy at a $y/h = 0.2$. Thus, it is realised that Van Driest damping indeed corrects the Smagorinsky constant to give better results close to the wall but has significantly lesser accuracies away from the wall as shown by the blue curve that is clearly closer to DNS than the green curve. As for cases 2 and 4, unlike the realisation for u'_{rms} in which case 4 showed less error than case 2, for v'_{rms} and w'_{rms}, it can be observed that case 2 has higher accuracy at higher y/h. Thus, upwind flux evaluation induces less error than using $C_s = 0.17$ for the rms fluctuations that are not in the flow direction.

3. Choice of settings for 64^3 case

Using the plots in Figure 1, the case with the highest accuracy can be deduced. Firstly from the plot of mean velocity U_{mean}, it can be noticed that case 1, 2 and 3 come close to the DNS results. This realisation does not change when looking at the fluctuation in flow direction u'_{rms}. However, when comparing the cases for fluctuations not in flow direction v'_{rms} and w'_{rms}, it can clearly be seen that case 5 is superior compared to cases 1 and 3. Thus, case 5 which corresponds to volume-averaged Smagorinsky with central flux evaluation was chosen for simulation with 64^3 mesh.

4. Estimation of Re_τ

Using the results from simulation of selected case 5 with 64^3 mesh, the velocity magnitude on an $x-z$ plane at $y = 0.1$ was visualised using contours as shown in Figure 2.

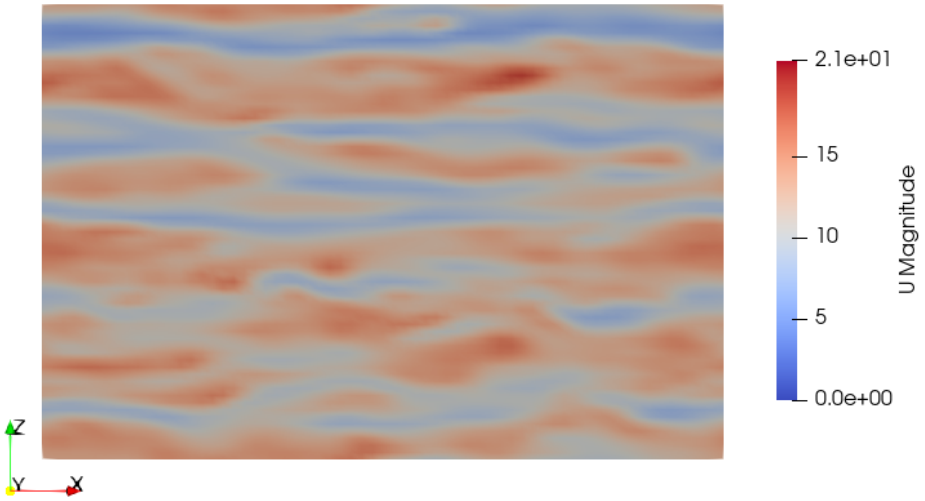

Fig. 2 Velocity magnitude on $x-z$ plane at $y = 0.1$ at the latest time

From the contour figure, streaks can be observed for this turbulent flow in a wall-bounded domain. These streaks are quasi-coherent structures and have alternating speeds, with high-speed streaks lying between the low-speed streaks. According to Kline and Robinson (1990), the low-speed streaks are found in the region $0 < y^+ \leq 10$ and thus, with a small value for y selected and presented in Figure 2, the presence of streaks are expected.

Since the low-speed streaks are spaced $z^+ = 100$ apart approximately, using the equation

$$z^+ = \frac{z_{\text{space}}}{\delta_\nu} \tag{4.1}$$

where z_{space} is the dimensional spacing in $z-$direction, δ_ν can be found and it is the viscous length scale which was found to equal to ν from (1.3).

It was deduced from Figure 2 that the value of z_{space} is roughly 0.5 and thus

$$\begin{aligned} \nu &= \delta_\nu \\ &= \frac{0.5}{100} \\ &= 0.005. \end{aligned} \tag{4.2}$$

Using (1.4), the approximate value of Re_τ is then found to be

$$\boxed{Re_\tau = 200}.$$

5. Analysis of eddy viscosity ν_{SGS}

To analyse the eddy viscosity from the simulations, contours on $x-$normal cutting planes at $x = 3$ are plotted for both 32^3 and 64^3 meshes as shown in Figure 3.

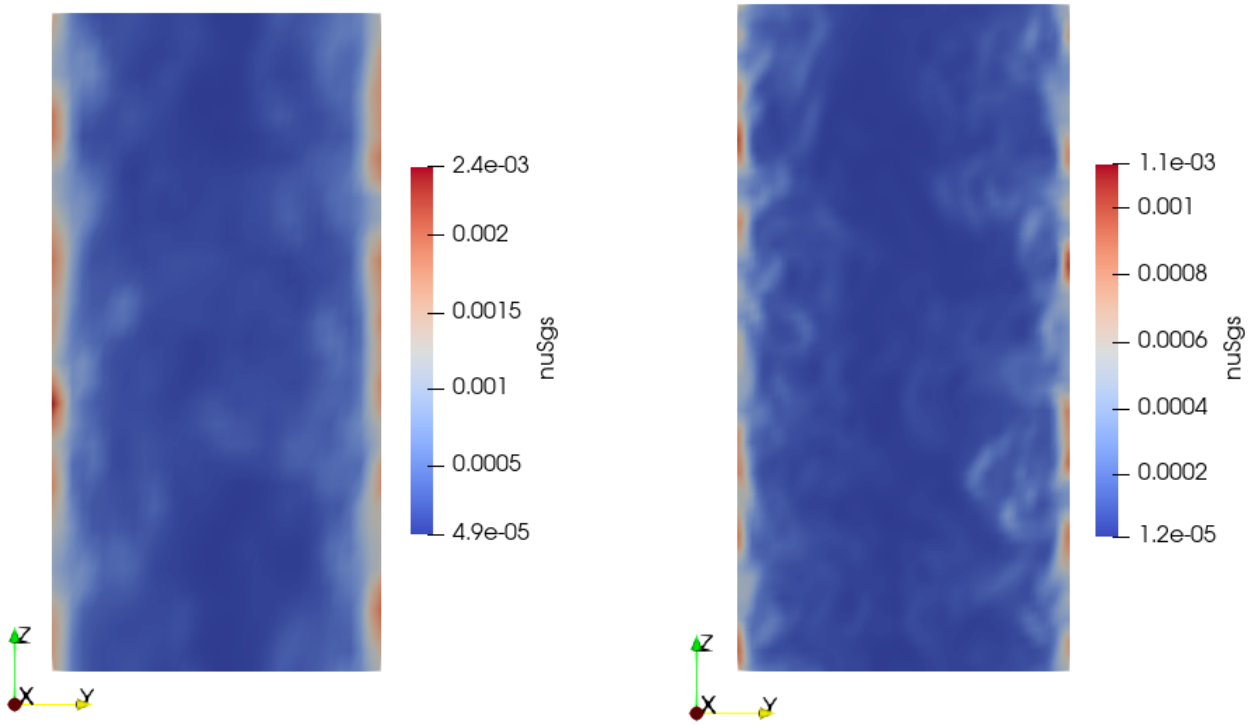

(a) 32^3 **mesh** **(b)** 64^3 **mesh**

Fig. 3 Eddy viscosity ν_{SGS} on $y - z$ plane at $x = 3$ at the latest time

It can be observed that for both meshes, the regions of maximum eddy viscosity are present close to the bottom and top walls, so at $y = 0$ and $2h$. This is as expected since the maximum eddy viscosity occurs at the walls for wall-bounded turbulent flows and is independent of the mesh resolution. However, the magnitudes in the two meshes differ. The maximum is 2.4×10^{-3} for 32^3 mesh while it is 1.1×10^{-3} for 64^3 mesh as it is shown in Figure 3a and Figure 3b respectively. Besides, the minimum is also much lower for the 32^3 mesh than the 64^3 mesh.

Eddy viscosity of Smagorinsky model is defined as

$$\nu_{\text{SGS}} = (C_s\Delta)^2 \sqrt{2\overline{S}_{ij}\overline{S}_{ij}},$$

where Δ is the filter width and

$$\overline{S}_{ij} = \frac{1}{2}\left(\frac{\partial \overline{u}_i}{\partial x_j} + \frac{\partial \overline{u}_j}{\partial x_i}\right).$$

Thus, the obtained results are as expected since the eddy viscosity scales with the square of filter width, resulting in the 64^3 mesh that has much smaller spacing between nodes, giving a smaller magnitude of the maximum eddy viscosity.

6. Analysis of vortex structures in late-time 64^3 solution

To visualise the vortex structures in a late-time 64^3 mesh solution, the isosurfaces of $Q = 100$ and $\lambda_2 = -100$ are produced as shown in Figure 4 and Figure 5 respectively at the latest time.

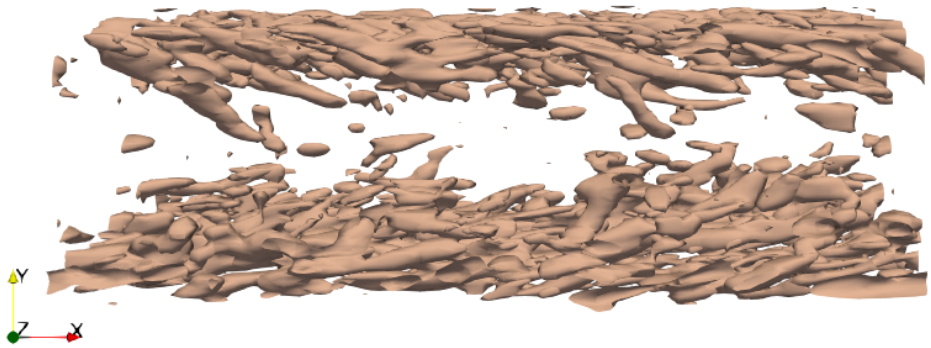

Fig. 4 Isosurface of $Q = 100$ for 64^3 mesh at the latest time

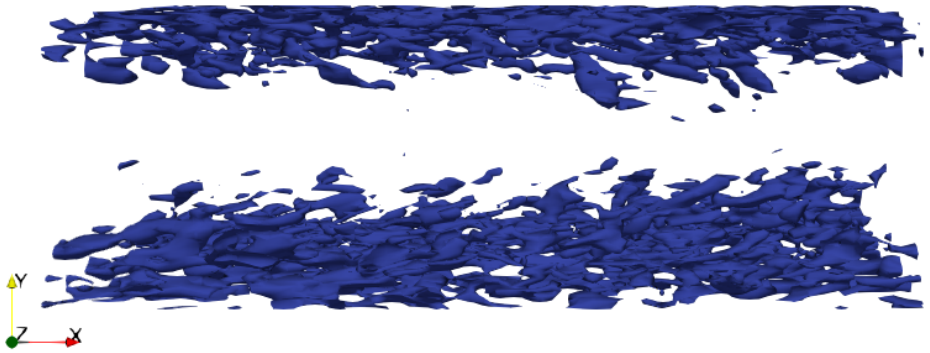

Fig. 5 Isosurface of $\lambda_2 = -100$ for 64^3 mesh at the latest time

The angles θ of the vortex structures with respect to the top and bottom wall were measured for as many structures as possible and the average value was found to be approximately

$$\boxed{\theta_{\text{average}} = 11.4^\circ}.$$

As for Piomelli's shifted corrections wall model, the estimation of shift in x is done for h_{wm} that corresponds to $y^+ = 50$ and 100. Using the value of δ_ν found in (4.2), we can calculate the corresponding values of h_{wm} for the required values of y^+ using

$$h_{wm} = y^+ \delta_\nu.$$

Thus, we have

$$h_{wm,y^+=50} = 0.25 \quad \text{and}$$
$$h_{wm,y^+=100} = 0.5.$$

For these two values of h_{wm}, the angles of the corresponding vortex structures with respect to the wall were analysed and the average values were found to be

$$\boxed{\theta_{h_{wm}=0.25} = 10.3^\circ}$$
$$\boxed{\theta_{h_{wm}=0.5} = 13.8^\circ}.$$

These two values then correspond to shifts in x of

$$\begin{aligned} x_{wm,y^+=50} &= \frac{h_{wm}}{\tan\theta} \\ &= \frac{0.25}{\tan(10.3^\circ)} \\ \boxed{x_{wm,y^+=50} &\approx 1.3757} \end{aligned}$$

and

$$\begin{aligned} x_{wm,y^+=100} &= \frac{h_{wm}}{\tan\theta} \\ &= \frac{0.5}{\tan(13.8^\circ)} \\ \boxed{x_{wm,y^+=100} &\approx 2.0356} \end{aligned}$$

respectively.

Using actual value of ν

However, it was found from the **transportProperties** file of OpenFoam that the actual value of $\nu = 0.00555$ which makes the actual value of δ_ν also 0.00555. Using this value, the values of h_{wm} are

$$\begin{aligned} h_{wm,y^+=50} &= 0.2775 \quad \text{and} \\ h_{wm,y^+=100} &= 0.555 \end{aligned}$$

which give shifts in x of

$$\begin{aligned} x_{wm,y^+=50} &= \frac{h_{wm}}{\tan\theta} \\ &= \frac{0.2775}{\tan(10.3^\circ)} \\ \boxed{x_{wm,y^+=50} &\approx 1.5270} \end{aligned}$$

and

$$\begin{aligned} x_{wm,y^+=100} &= \frac{h_{wm}}{\tan\theta} \\ &= \frac{0.555}{\tan(13.8^\circ)} \\ \boxed{x_{wm,y^+=100} &\approx 2.2596} \end{aligned}$$

respectively.

7. Observation of hairpin vortices

Upon reviewing the isosurfaces for $Q = 50$ and $\lambda_2 = -50$ for every timestep of the 64^3 mesh, it was concluded that there are no coherent vortex structures that can confidently be labelled as hairpin vortices. A couple of structures that were deemed to be coming closest to the hairpin vortices are presented in Figure 6 and Figure 7 and circled in red.

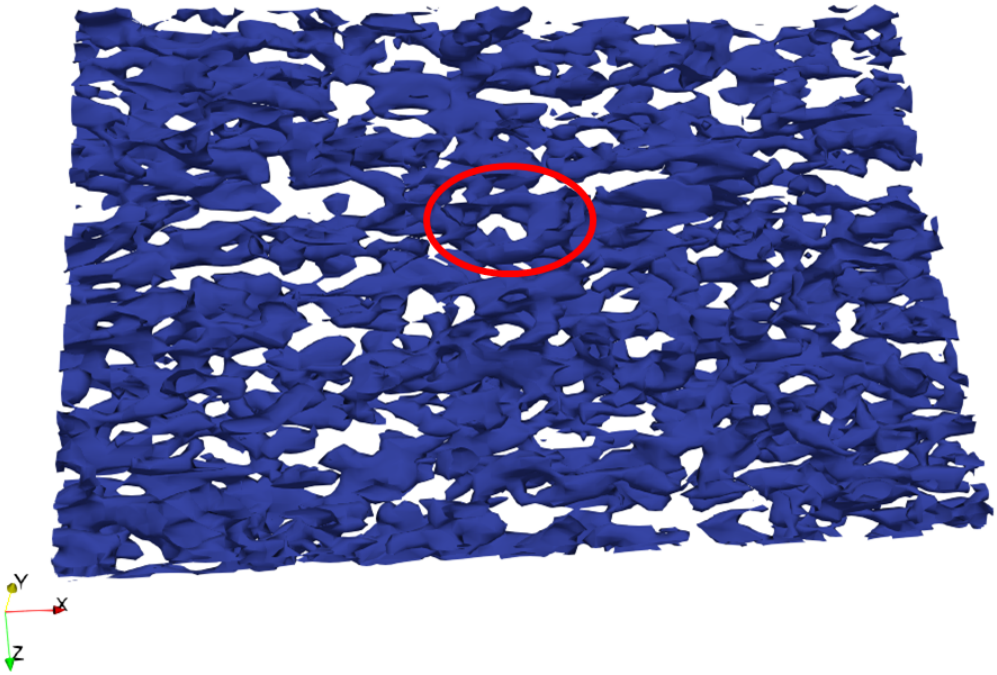

Fig. 6 Isosurface for $\lambda_2 = -50$ at the first timestep

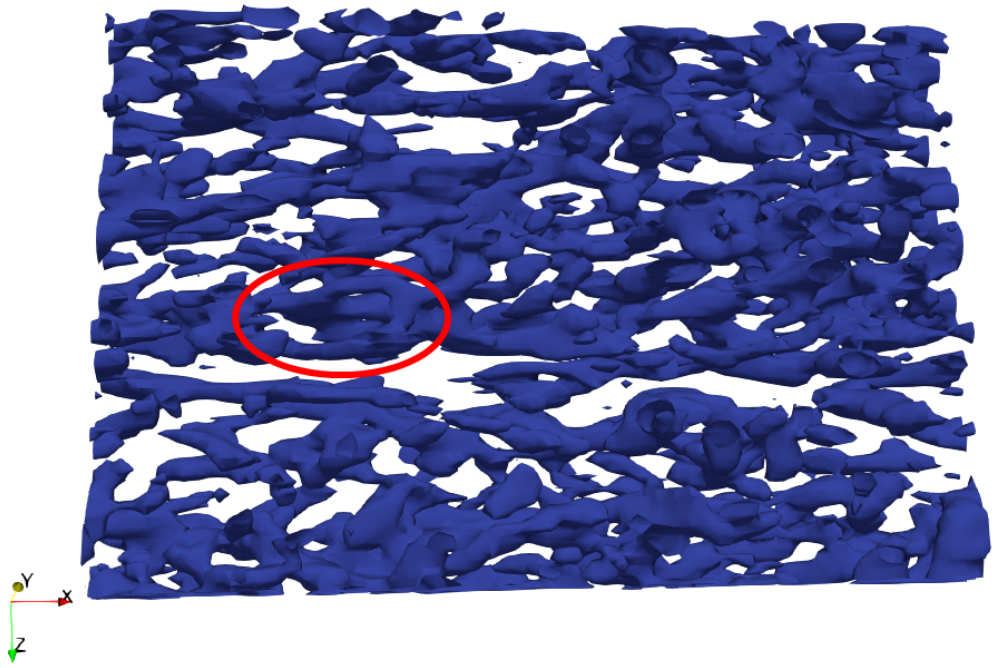

Fig. 7 Isosurface for $Q = 50$ at the latest time

However, they are still far from a typical hairpin vortex structure and since each of the two presented structures lives among the other structures alone, it cannot be said that they are hairpin vortices since hairpin vortices usually occur in packets.

Since these hairpin vortices typically occur in turbulent flows with $Re_\tau < 590$ given by Eitel-Amor et al. (2014), with the value $Re_\tau = 180$ found in section 4 for this specific turbulent channel flow, the magnitude of Re_τ is not the reason for the absence of hairpin vortices. It was also realised for the isosurfaces at every time sequence that the vortex structures do not seem distinct and are somewhat connected to one another, making it difficult to distinguish between each elementary vortex structure. Thus, it can be concluded that the absence of the hairpin vortices is due to the low resolution of the simulation.

References

Georg Eitel-Amor, O. Flores, and Philipp Schlatter. Hairpin vortices in turbulent boundary layers. *Journal of Physics, Conference Series*, 506(1):012008–, 2014. doi: 10.1088/1742-6596/506/1/012008. QC 20140625.

S. Kline and S. Robinson. Turbulent boundary layer structure: Progress, status, and challenges. 02 1990. doi: 10.1007/978-3-642-50971-1_1.